Institute of Visualization and Interactive Systems

University of Stuttgart
Universitätsstraße 38
D–70569 Stuttgart

Bachelorarbeit Nr. 159

Imposters for Particle-Based Datasets

Patrick Wickenhäuser

Course of Study:	Softwaretechnik
Examiner:	Prof. Dr. Thomas Ertl
Supervisor:	Dr. Guido Reina, Dr. Peter Rautek, Prof. Dr. Markus Hadwiger
Commenced:	09. Juli 2014
Completed:	09. Januar 2015
CR-Classification:	I.3.3, I.3.8, I.4.3, I.4.8

Kurzfassung

Viele partikel-basierte Datensätze bestehen aus mehreren Millionen von Partikeln. Diese stammen meist aus Molekulardynamic-Simulationen. Aktuelle Visualisierungstechniken sind nicht in der Lage Datensätze dieser Größe konsistent über alle Skalen hinweg zu repräsentieren. Sie produzieren entweder stark vereinfachte Darstellungen oder sind anfällig für *Aliasing*, aufgrund zu niedriger Abtastraten. Diese Arbeit stellt eine neue Visualisierungstechnik vor, die die Partikeloberflächen konsistent und mit hoher Genauigkeit repräsentieren. Diese Technik basiert auf *normal distribution functions* und *impostern*. Mit ihr konnten Visualisierungen von Schockwellen in Aluminiumgittern produziert werden, die mit aktuellen Visualisierungstechniken nicht erreichbar waren.

Abstract

Many particle-based datasets produced by molecular dynamics simulations consist of millions of particles. Current visualization techniques are incapable of representing those large-scale datasets consistently across all scales. They either produce overly-smooth representation or are prone to aliasing due to under-sampling. This work introduces a technique that captures the micro-scale surface features accurately and is able to represent the complex local illumination behavior of hundreds of particles in a single pixel-footprint. This scale-consistent technique allows for an overview that is resistant to aliasing and true to the micro-scale surface. This technique produces visualization of shock waves that could not be seen before without dedicated visualization methods. It can be applied to any opaque particle glyphs and BRDF model.

Contents

1 Introduction

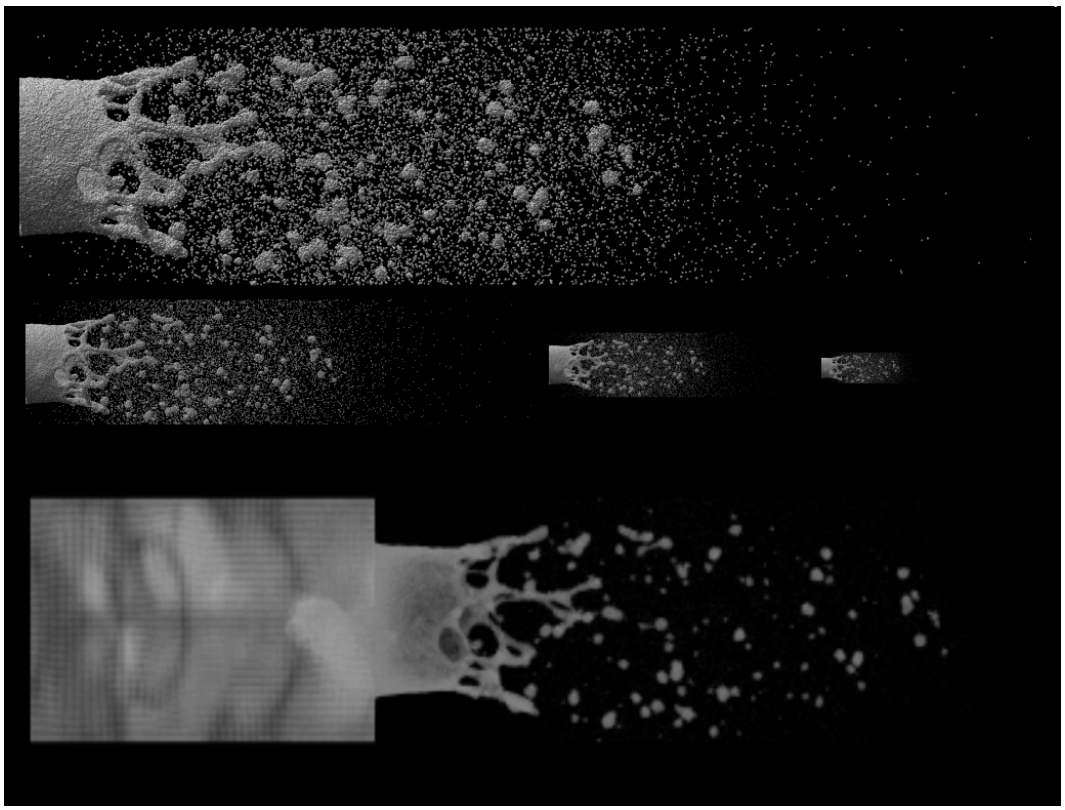

Figure 1.1: Visualization of particle-based data at multiple scales using the technique introduced in this work.

Large-scale particle-based data is getting increasingly important due to the increasing computational resources available. This allows scientists in the field of molecular dynamics to conduct simulations with an ever-growing amount of particles. The scale of a simulation is important to capture relevant effects that cannot be captured with too few particles because of too infrequent interactions. A visualization of a single time step of such a simulation can be seen in figure 1.1. Visualization plays an important role to find errors, check the results against the model, convey information to other people and even laymen in the field. Or possibly even to find unexpected features and areas of interest not previously observed.

A possible model of representing the particles is further described in section 1.1. It represents each particle as a perfectly round sphere, hereinafter referred to as the sphere glyph model. The relevance of the sphere glyph model in the field of thermodynamics has been confirmed by Prof. Dr. Jadran Vrabec, who has been approached during this work and sent prototypical images to. The radius corresponds to the Van-der-Waals-Radius used in molecular dynamics simulation therefore is still important for visual verification of simulations. This model is used throughout this work, however the methods introduced are not restricted to this particular glyph model but can be applied to any surface model consisting of fully opaque surfaces.

Current graphics hardware is easily capable of rendering millions of particle glyphs with interactive frame rates. The increasing amount of particles brings new challenges as visual clutter, caused by under-sampling, hides areas of interest. As a result scale-invariance of the visualization plays an important role to allow a meaningful overview of the dataset from afar that is true to the actual micro-scale features.

1.1 Sphere Glyph Model

Each particle is represented by a perfectly round sphere described by its position and radius. The sphere does not represent the orbitals of atoms, that are not necessarily round, but the spherical force fields used in molecular dynamics simulations. The exact radius and position of each particle can been seen, in contrast to direct volume rendering (section 2.1.3) where usually only the density of the particle distribution is represented. There are more elaborate methods for rendering volumetric data. One approach uses ray casting of radial basis functions and is able to capture particle surfaces well [KWN+14].

This work focuses on local illumination of fully opaque glyphs. The glyph model has been extended with ambient occlusion in [GKSE12] to enhance depth perception and accentuate discontinuities to allow the user to recognize larger-scale structures through low frequency lighting effects. Neither scattering nor phase functions are addressed in this work.

This is a very simple model in the context of small datasets consisting of only hundreds of particles though rendering large-scale data are a challenging problem. The ground truth is not known and expected to have highly complex shading on a large-scale similar to the micro-facet model [CT82] which consists of large numbers of tiny perfectly specular planar surfaces, referred to as microfacets, that by themselves are very simple but together form complex shading behavior once observed from afar. Therefore an

essential part of this work is the derivation of a technique capable of computing the ground truth.

1.2 Problems using the Example of a Laser Ablation Dataset

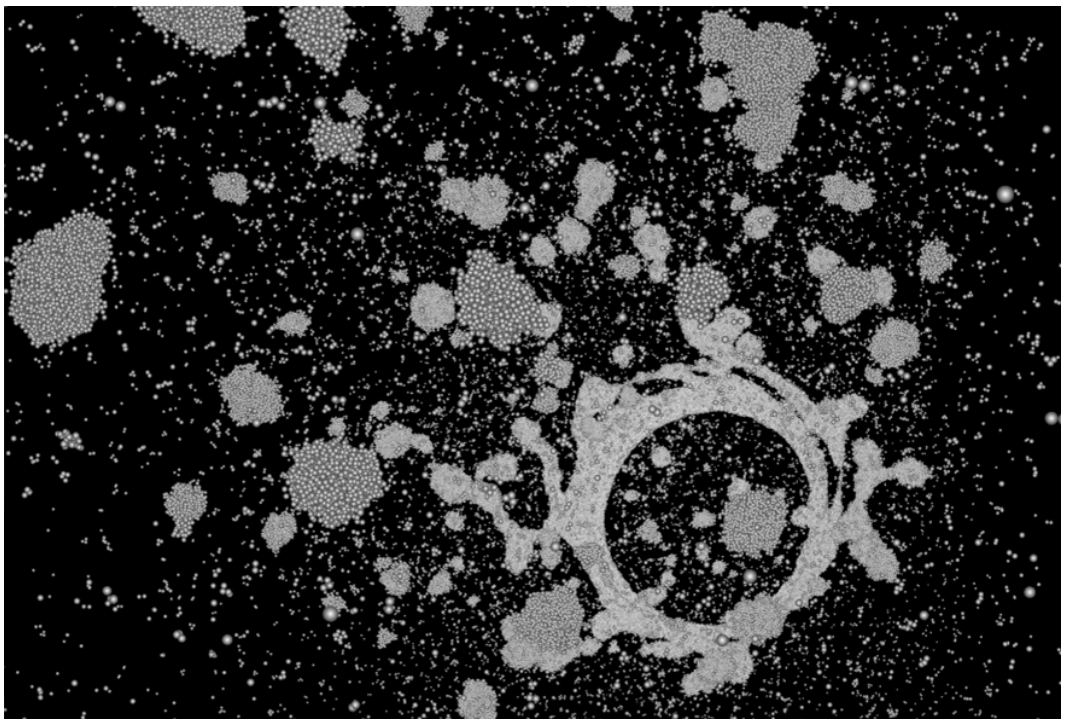

Figure 1.2: Aliasing of particles far away due to undersampling.

Visualization of this sort of datasets is challenging due to occlusion and visual clutter. A human is only able to interpret a small subset of particles visualized as sphere glyphs at once. To give the user an overview to select a smaller area of interest a representation is required that preserves the small-scale features of the dataset even when viewed from afar.

The representation has to be resistant to aliasing and numerical errors that potentially introduce non-existing or hide features. During this work there were several discussions about whether some visible features on the particle surface are actually originated from the particle data or are artifacts of the visualization. Manual adjustment of the camera or clipping can be used to verify an observation, though this is counter-intuitive and time-consuming.

The current state-of-the-art visualization technique for particle glyphs is GPU-based

direct particle rendering introduced in [Gum03] (section 2.1.1). This approach is extremely useful on small scales but suffers from heavy aliasing and a lack of consistency across different scales due to under-sampling. An image generated using direct particle rendering can be seen in figure 1.2. The particles close to the camera are very well captured using this technique, nevertheless particles more distant to the camera are extremely noisy. Only the outline of the more distant particle surfaces can be seen. The structure on the surfaces are completely hidden by noise.

1.3 Datasets

This work uses the following datasets.

- Laser ablation simulation dataset. This dataset is a single time step of a laser ablation simulation consisting of more than 48 million particles. Sometimes only the particles shot out of the aluminium block are used, hereinafter referred to as the crown of the laser ablation.
- Cross ablation simulation dataset. Another single time step of a laser ablation simulation is used. The laser in this simulation moves over time to cut a cross in the block of aluminium. It consists of 562500 particles.
- A smaller molecular dynamics simulation dataset consisting of 23328 particles is used.
- Several synthetic datasets are generated. They mostly consist of millions of particles that together form a spherical surface. Those spheres have different repeating small-scale patterns of only a few particles to examine the effect of different micro-geometries on the large-scale shading behavior.

1.4 Scales

During this work the scales are categorized into micro, meso and macro scale. Instead of a global scale of a certain dataset, the scales referred to are defined by the amount of particles per pixel footprint.

- Micro: a fraction of a particle per pixel footprint.
- Meso: between 1 and 10 particles per pixel footprint.
- Macro: at least 10 particles and a lot more.

The categorization is motivated by the quality achieved using direct particle rendering (section 2.1.1) that directly depends on the number of samples taken per particle. Direct particle rendering is able to represent particles in the micro-scale well using ray casting, which calculates the nearest intersection of the view ray and the particle surface. The lighting of the pixel footprint covered by the view ray is approximated by shading a planar surface patch oriented towards the normal sampled at the intersection point. A large number of planar approximations are required to accurately represent the curved surfaces of particles.

The number of samples can be increased using super-sampling to capture a higher amount of particles. However increasing the number of samples quickly becomes extremely costly. The definition of the meso-scale is based on the amount of particles that can be rendered with interactive frame-rates using super-sampling. Some of the datasets targeted by this work have several hundreds of particles per pixel footprint. The macro-scale therefore includes any amount of particles per pixel footprint that is too expensive to render using super-sampled direct particle rendering.
The targeted scale-invariant visualization method has to be capable of representing all of these scales accurately and consistently.

1.5 Goals

This section discusses the attributes demanded of the visualization to allow effective visual analysis of the targeted datasets.

The importance of countability can be observed when comparing clusters of particles with each other. It is important to distinguish near and / or large particles from clusters of smaller or farther particles, even if they have the same on-screen footprint. Such a situation is illustrated in figure 1.3.

Complex lighting of rough surfaces due to the micro-structures of materials can be observed in nature. Such rough surfaces and micro-geometry have been studied in [YHJ+14]. They show how complex lighting can emerge from small-scale features that by themselves have very simple lighting models, in this case perfectly reflecting planes called micro-facets. See section 3.2 for further experiments.

This work offers the following contributions:

- The ground truth of the minification problem of representing large-scale data on small screen footprints under the assumption of fully opaque glyph models without the restriction of a fixed glyph BRDF model.

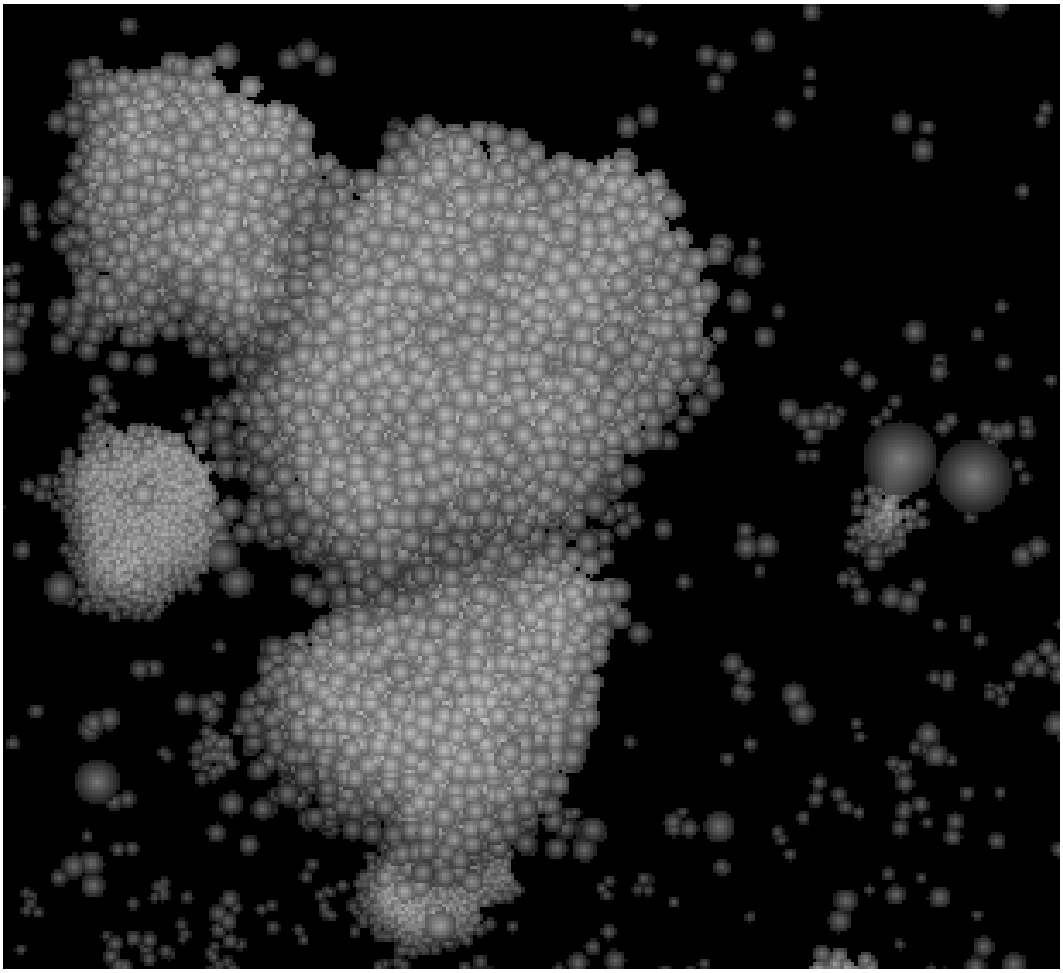

Figure 1.3: Clusters of particles with different distances to the camera.

- A scale-invariant representation that preserves the small-scale features and appearance of the underlying glyphs on all scales. Those features include small-scale cracks and dislocations in a material sample that result in complex anisotropic shading behavior and the preservation of rough surfaces important to convey information about the number and regularity of particles. The technique should be resistant to numerical problems and aliasing.

2 Background

This chapter summarizes the fundamentals and related work used throughout this thesis.

2.1 Fundamentals

This section explains some well studied techniques and basic concepts required for the following chapters.

2.1.1 Direct Particle Rendering

Several techniques for rendering particles directly, using GPU ray-casting, exist. One of them is based on the concept of splatting illuminated ellipsoidal glyphs [Gum03]. Splatting is an object-space algorithm in contrast to computing image-space intersections of rays and particles. A similar technique has been applied to large-scale particle-based data [GRDE10]. These techniques based on splatting GPU ray-casted glyphs are referred to as direct particle rendering in this work. An own implementation of this technique is used throughout this work.

2.1.2 Imposters

Imposters have been introduced by Shade et al. [SLS+96]. This approach renders geometry to an image with a fixed view direction, perspective and shading. Later this image can be used to avoid rendering the actual geometry by only drawing its image instead. The precomputed image is only able to replace the actual geometry if neither the view direction or perspective nor shading has changed. To capture any occurring changes the imposter has to be repeatedly recomputed. Some variations of classical imposters store geometrical information to compute the shading in a deferred shading pass to account for changing lighting without the need of recomputation.

2.1.3 Volume Rendering

Volume rendering is a class of techniques for rendering volumetric data with various applications. These techniques are mostly used for rendering scalar fields containing density values. Some methods that produce such scalar fields are MRI or CT that measure real world data used in medicine and engineering. Also some simulations produce scalar fields often visualized using volume rendering. Particle-based data can also be transformed into a scalar field by splatting the particles density values using an appropriate kernel. Most techniques implement shading based on the density gradient.

2.1.4 Normal Distribution Function (NDF)

The normal distribution function (NDF) was introduced by Alain Fourier [Fou92]. NDFs are two-dimensional functions defined on each surface area of the sample. The function returns the density of a given normal vector on the hemisphere over the local tangent frame. Below the hemisphere (on the backside of the surface) the NDF returns zero for each direction. It does not contain any information about where the normal vectors are located within that area.

These functions are important for shading as they are able to statistically represent micro-scale surface features. The density of normal vectors given by the NDF enables independent shading and accurate filtering of each normal vector with a simple illumination model (BRDF), like Blinn-Phong [Bli77], which results in complex shading. The evaluation of the BRDF of each normal vector is a convolution of the NDF with the BRDF which results in the so called effective BRDF. This convolution can be done upfront, reducing the evaluation of each normal vector independently to a single evaluation of the effective BRDF.

Since NDFs are probability density functions they can be filtered linearly. Linear filtering of normal vectors themselves however is not possible. As a result NDFs can be used efficiently with standard mip mapping which is helpful for scale-invariant representations. Normal distribution functions are used in this work because of their ability to capture the complex effective BRDF of micro-scale particles and their ability to be used with standard mip mapping.

Normal distribution functions are often illustrated as 2D images. The x, and y-coordinate represent the normal vector coordinates from -0.5 to 0.5 in tangent frame space. Since all normal vectors within the circle around the center of the image are normalized the third coordinate can be calculated using the knowledge of the length.

Figure 2.1: A highly detailed normal distribution function illustrated as a two-dimensional image taken from [YHJ+14].

All vectors outside of the circle are invalid thus their probability should always be zero. The grayscale intensity represents the density of the given normal vector. An illustration of a highly detailed NDF can be found in figure 2.1 [YHJ+14]. The intensity values are transformed into a visible range according to the maximum and minimum intensity. A measurement of a real world NDF using a camera and a material sample has also been conducted [YHJ+14].

2.2 Related Work

This section summarizes related work in the area of multi-scale rendering.

2.2.1 Seamless Visual Abstraction of Molecular Surfaces

Parulek et al. [PRV13] presented a level-of-detail rendering approach that uses a combination of multiple visualization techniques. The particle surface is rendered in the form of solvent excluded surfaces, van der Waals spheres and Gaussian kernels depending on the current scale. The shading model is chosen to be diffuse with a black outline on the edges to highlight discontinuities. Together with low-frequency ambient occlusion this visualization technique leads to good depth perception. The three different surface models are blended linearly using the distance from the camera to hide the transition in-between.

This related work aims at giving the user fast and meaningful visualizations but changes models throughout different scales. An accurate visualization of particles as small as a pixel is not target using this technique. Our work attempts a similar approach to represent large-scale particle-based data using smoothly blended visualization techniques, in our case direct particle rendering and mip mapped volume rendering.

2.2.2 Frequency Domain Normal Map Filtering

Frequency Domain Normal Map Filtering was introduced by Han et al. [HSRG07]. They have developed a theoretical framework for filtering high resolution normal maps using approximations of the resulting normal distribution functions (NDF) using spherical harmonics or von Mises-Fisher distributions. Additionally they have shown how those distributions can be used directly for computing the shading result of a normal mapped surface analytically. Spherical harmonics are well suited when targeting low-frequency BRDFs while von Mises-Fisher distributions are better suited for high-frequency BRDFs. Their representation is accurate across many scales but limited to normal vectors on a common tangent frame.

Filtering of normal maps is relevant to this work since the introduced technique samples the particles' surface normal vectors into high-resolution normal maps. Those normal vector samples have too large memory requirements to be stored on the GPU let alone be sampled in real-time during shading thus accurately filtering of the high resolution samples to a more compact representation is an essential part of this work.

2.2.3 Sparse PDF Maps

Sparse PDF maps [HSB+12] enable accurate and efficient evaluation of color mapping and non-linear filters such as the edge-preserving local Laplacian filter. The approach sparsely approximates the probability density functions (PDF) of pixel neighborhoods using continuous functions. Multiple output resolutions (scales) are addressed using mip-mapping. Each mip-level is separately approximated based on the original data using differently sized spatial pre-filters. The sparse approximation results in memory consumption in the same order of the original image. Their work shows how maintaining the histogram throughout the mip-levels is important for scale-consistent filtering of images. During filtering only the output resolution mip-level is required, making the approach feasible for gigapixel images.

Their sparse approximation uses Gaussian mixture models obtained using matching pursuit. Prior to fitting the two-dimensional image is lifted to the three-dimensional (space x range) domain to exploit neighborhood not only in the spatial but also in the range domain. This a computationally expensive process but they have shown that the error of the approximated data is very small.

Sparse pdf maps have recently been extended to volumetric data [SKMH14], called sparse PDF volumes that improve the scale-consistency of color mapping on mip-mapped volumes. Sparse pdf maps are related to this work since local illumination is a non-linear operation on the particle surface normal vectors which suffers from similar inconsistency artifacts on different scales as applying color mapping to downsampled density values does.

2.2.4 LEAN and LEADR Mapping

Linear efficient and antialiased normal mapping (LEAN) [OB10] is a technique for efficient and aliasing resistant filtering of normal mapped surfaces. Their approach starts by representing the normal vectors of the finest resolution level by isotropic Gaussians centered on the normal vectors. The Gaussians are stored using 2x2 covariance matrices. Using this representation downsampling for mip mapping can easily be done by linearly filtering of the seconds moments. The resulting downsampled Gaussians are not necessarily isotropic anymore. LEAN mapping makes assumptions about the BRDF used and therefore restricts its use to certain BRDFs.

LEADR mapping [DHI+13] is based on LEAN mapping but extends its concepts further to displacement mapped surfaces and show the application of accurate normal map filtering in environment lighting. Their filtering uses 3x3 covariance matrices.

However this still requires the tangent frame of the underlying surface which does not exist when rendering non-intersecting particles.

3 Experiments

In this chapter the well-studied techniques of direct particle rendering (section 2.1.1) and mip mapped volume rendering (section 2.1.3) are applied to our problem in order to inspect how well they perform on particle-based data and the sphere glyph model. Subsequently a ground truth model is derived to evaluate whether the inspected techniques are able to represent the data appropriately.
Finally a new technique based on normal distribution functions [Fou92] and classical imposters [SLS+96] is derived and evaluated.

3.1 Combination of Volume and Particle Rendering

The obvious approach to visualize large numbers of particles is volume rendering. Particle-based data can be transformed into volumetric data by splatting the particle densities into a density scalar field on which standard volume rendering is applied. Different scales are addressed using standard mip mapping. In addition to volume rendering, particles close enough to the camera are individually rendered using direct particle rendering. Both representations are blended smoothly.

3.1.1 Implementation

Firstly this approach needs to compute the density scalar field and density gradient vector field used during volume rendering. The particles are transformed into 3D texture space within a range of 0 to 1, while maintaining the aspect ratio of the bounding geometry. Then the density values are splatted using the Gaussian kernel and the density gradients are splatted using the derived Gaussian kernel.

Rendering of the two techniques is performed independently in separate passes. The volume rendering pass uses front to back composition therefore the view ray's entry point into and exit point out of the domain have to be known per fragment. To find the exit points of the rays, the object space positions of the domain bounding geometry back face are rendered into a render target as illustrated in figure 3.1. The entry points are computed similarly by rendering positions of the domain bounding

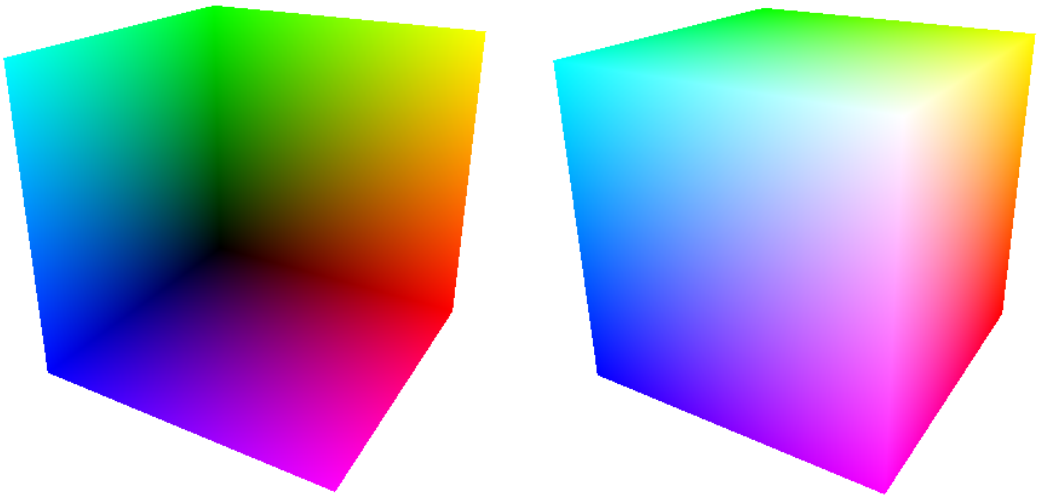

Figure 3.1: Front and back face of the bounding geometry. The colors represent the object space positions used for ray calculation.

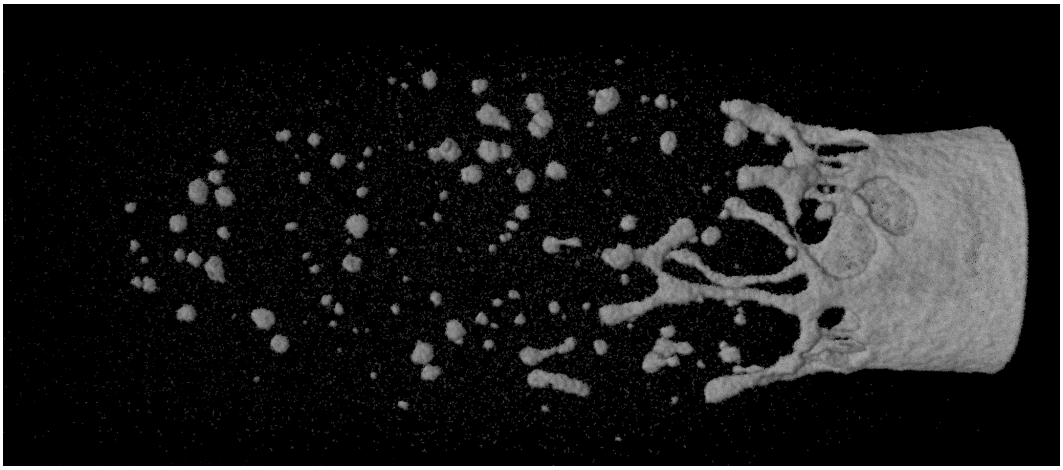

Figure 3.2: Renderings using a combination of volume rendering and direct particle rendering

geometry front faces. Special care has to be taken if the camera is located within the boundary geometry, in which case the front face is clipped by view plane, resulting in a gap in the front faces. This case is addressed by clipping the bounding geometry front face before rendering and filling any resulting gap. Obviously there are better-suited, more tightly enclosing boundary geometries than axis aligned bounding boxes that could be used instead to skip empty spaces.

Finally a shader applied to the bounding geometry front faces calculates the line segments using the entry and exit points then steps through the volume along the line

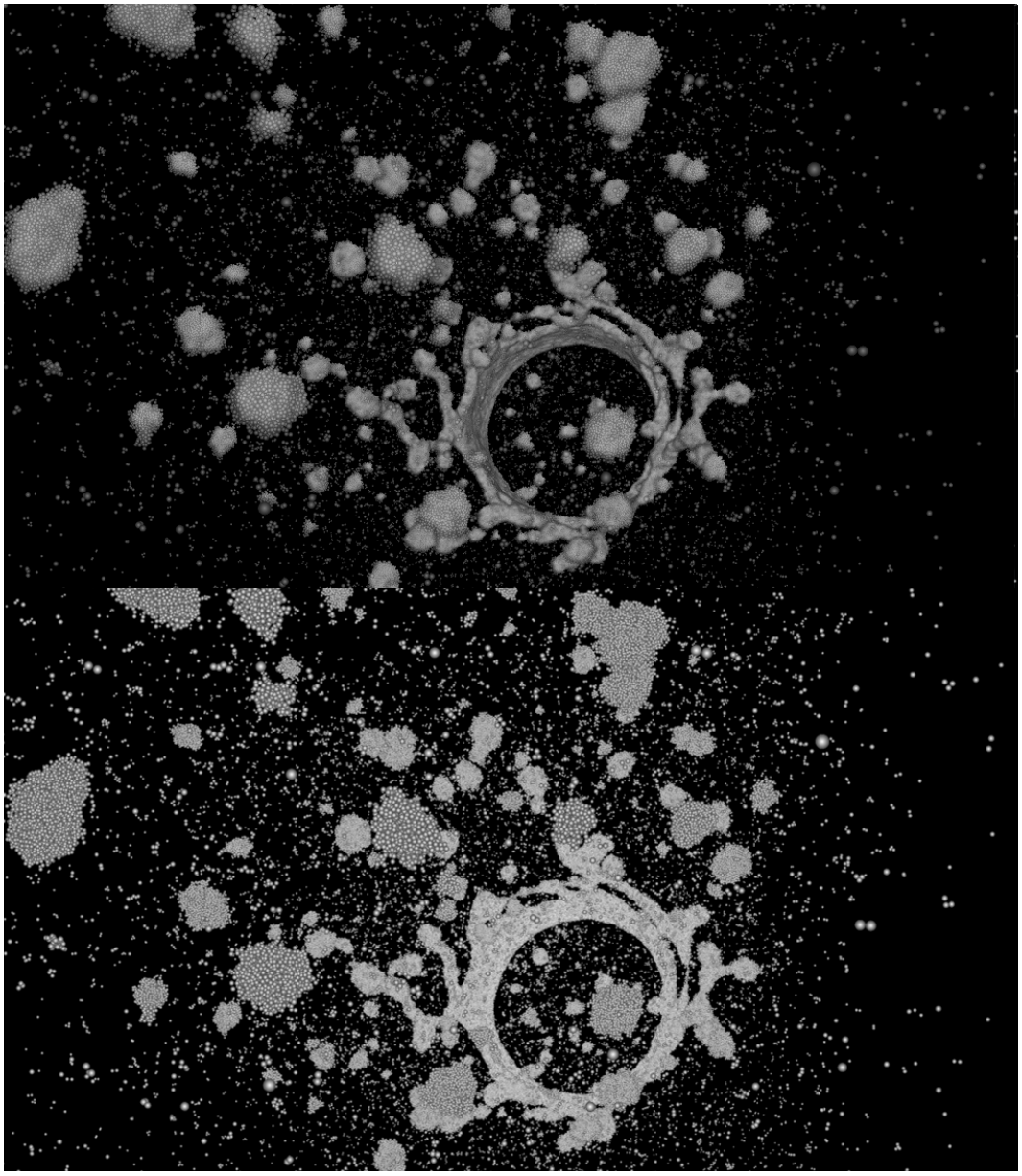

Figure 3.3: Comparison of direct particle rendering (bottom) and the combination of volume rendering and direct particle rendering (top).

segment, sampling the density scalar field and density gradient vector field in regular

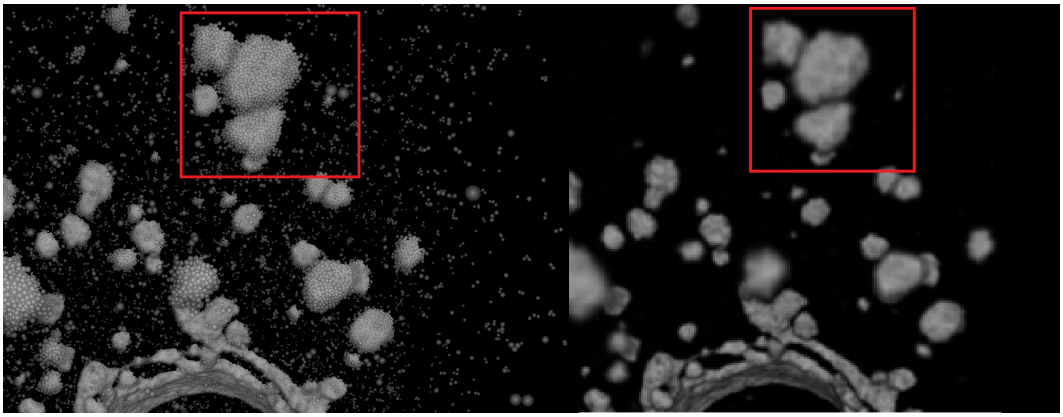

Figure 3.4: Comparison of blended rendering and volume rendering only of particles splatted into a density scalar field. A problematic area is highlighted in red where differently sized clusters of particles are accumulated to overly smooth clusters causing a loss of comparability between the clusters as well as depth perception.

intervals. Each sample is shaded and composited with the overall fragment results using equation 3.1 [IKLH].

$$c_{i+1} = (1 - o_i) * c + c_i \qquad o_{i+1} = (1 - o_i) * o + o_i \tag{3.1}$$

Where c_i is the current and c_{i+1} the resulting composited color after step i. Similarly o_{i+1} and o_i denote the composited opacity values. c and o are the color and opacity value of the current sample respectively.

Direct particle rendering is independently rendered into a render buffer. Particles always have at least the size of one pixel. Finally this method combines both visualization methods into a single image.

3.1.2 Blending

The two independent visualizations of the same data are combined using a weight calculated during particle rendering based on the screen footprint of the particle. It can be used as a measure to find out which of both methods visualizes the data more appropriately. As the particle footprint decreases sampling normals on the particle surfaces are increasingly prone to aliasing therefore the mixture increasingly tends towards volume rendering. The outline of a particle is used as a stencil for the blending

between both visualizations since volume rendering tends to over-smooth the actual particles.

3.1.3 Results

Low-frequency lighting of volume rendering combined with the high-frequency outlines of direct particle rendering produce good visual results. See figure 3.2 for a rendering using this technique and figure 3.3 for a side-by-side comparison with direct particle rendering.
Aliasing artifacts are avoided by using the low-frequency lighting of a coarse iso-surface as soon as undersampling would occur in direct particle rendering.
The extension of direct particle rendering with volume rendering allows the user to see meso-scale structures on top of the particles. Although this allows for a better high-level overview, the blending of the two substantially different visualizations of, on the one hand smooth iso-surfaces and on the other hand non-intersecting particles is undesirable. The differences between the two approaches are hidden by the smooth transition and mip mapping.

The amount of voxels required to appropriately capture individual particles as non-intersecting spheres is not only related to how densely a volume is populated but also to the size of the smallest particle in that volume. Memory requirements and sampling rates required for datasets consisting of millions of tiny spheres is expensive without smoothing particle surfaces with neighbors to larger clusters suggesting non-existing continuous transitions between non-intersecting particles. This results in a loss of information like the ability to distinguish or count individual particles which is important for the interpretation of simulations (section 1.5). The problem of the unwanted smoothing is shown in figure 3.4.

Mip mapping requires adjusted transfer functions for different mip levels requiring manual adjustment or a more elaborate representation like sparse PDF maps [HSB+12] (section 2.2.3) to allow consistent transfer functions throughout all scales. However even under the assumption of a scale-consistent method of applying transfer functions on the density scalar field the problem of an overly smooth representation remains.
Blending volume rendering with direct particle rendering is able overcome this problem to a certain extent by reintroducing high frequencies but itself suffers from aliasing and does not help in the macro-scale.

A more subtly problem of volume rendering is the lack of proper occlusion of particle surfaces during composition while stepping along the ray. The composition (equation 3.1) does neither account for occlusion nor the particle locations within a voxel

but only uses the whole voxel's density value for composition. This does not account for dislocations along a regular grid where partially occluded surfaces create shading effects not captured in the density scalar field.

Overall this concludes the need for further investigations to find the ground truth rendering of high-frequency micro-geometry across all scales and find a method that is able to represent the data accurately and consistently.

3.2 Offline Ground Truth Renderings

The assumed opaque sphere glyph model (section 1.1) is expected to produce more complex shading on a macro-scale than the density gradient used in the prior section 3.1 is able to capture. To support this hypothesis an experiment is conducted using offline super-sampled ray casting.

3.2.1 Approach

The goal is to answer the question if the simple sphere glyphs with uniformly distributed normal vectors can even lead to complex shading. The effect is expected to be caused by occlusion, therefore reducing the particle radii should reduce the effect of occlusion leading to more uniformly distributed normal vectors, while increasing the radii should lead to more accentuated surfaces. The effects of micro-geometry on the macro-shading is examined using synthetic datasets of spheres consisting of particles with different repeating surfaces on a scale in the order of a single pixel-footprint.

3.2.2 Setup

The offline rendering is done using PovRay 3.7. It is setup to calculate the first hit and simple Phong shading (local illumination). There are no shadows, ambient occlusion or any secondary rays. The target resolution is 8192x8192. High sampling rates are important accurately capture the individual spheres.

To be able to observe the behavior of different target resolutions the full resolutions image is downsampled using a box filter reducing blocks of 2x2 pixels into a single pixel. The image size is iteratively reduced by half in both dimensions until the target output resolution of 256x256 pixels is reached.

3.2.3 Results

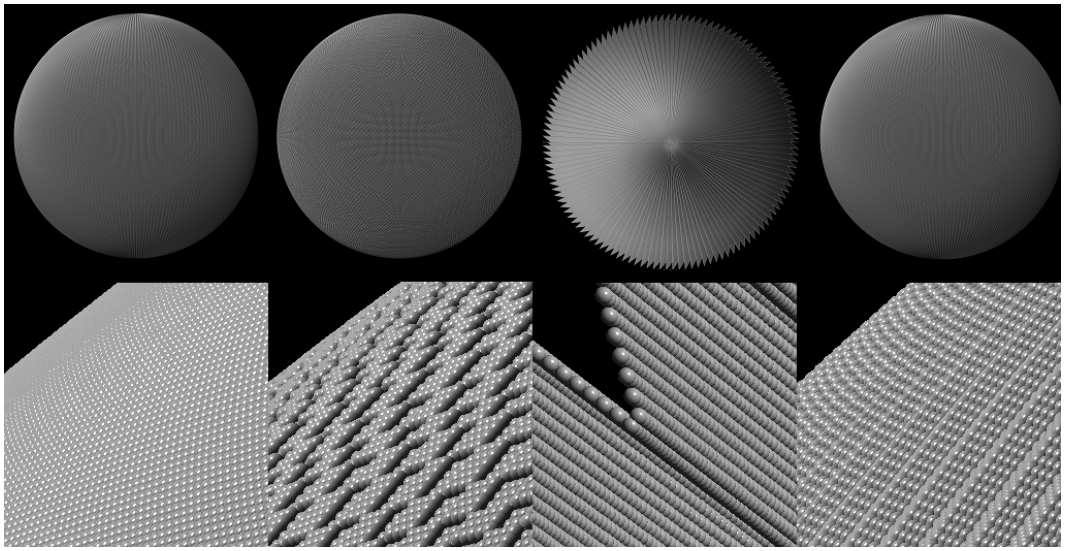

Figure 3.5: Comparision of macro-shading of spheres with different micro-geometries and a close up view below. Smooth, Checkerboard, Saw tooth and V Groove (from left to right)

Differences in the macro-scale shading behavior of different micro-geometries can be observed in figure 3.5. Standard mip mapped density gradients (section 2.1.3) used in volume rendering chooses the mip level according to the output resolution leading to only as many density gradient samples as the image space footprint. This is an overly smooth representation for micro-geometry and would lead to loss of those effects caused by the micro-geometry observed that lets the checker board sphere appear more flat than the smooth sphere for example. Also the anisotropic shading of the saw tooth hemisphere could not represented on a macro-scale.

3.3 Conclusion

Experimental renderings in section 3.1 show that the micro- and meso-scales (section 1.4) are covered well by direct particle rendering and volume rendering respectively. However at a macro-scale direct particle rendering suffers from heavy aliasing due to under-sampling. This concludes the need for a new approach to solve the minification problem that arises in the macro-scale.

4 NDF Imposters

In this chapter the concept of a scale-invariant normal distribution function rendering technique is introduced and applied to classical 2D imposters (section 2.1.2). This approach is aimed to accurately represent the macro-scale (section 1.4) in which a large amount of particles occupy the footprint of a single pixel. In this case, super-sampling would require too many samples to achieve real-time rendering performance on current graphics hardware.

4.1 Normal Distribution Rendering Concept

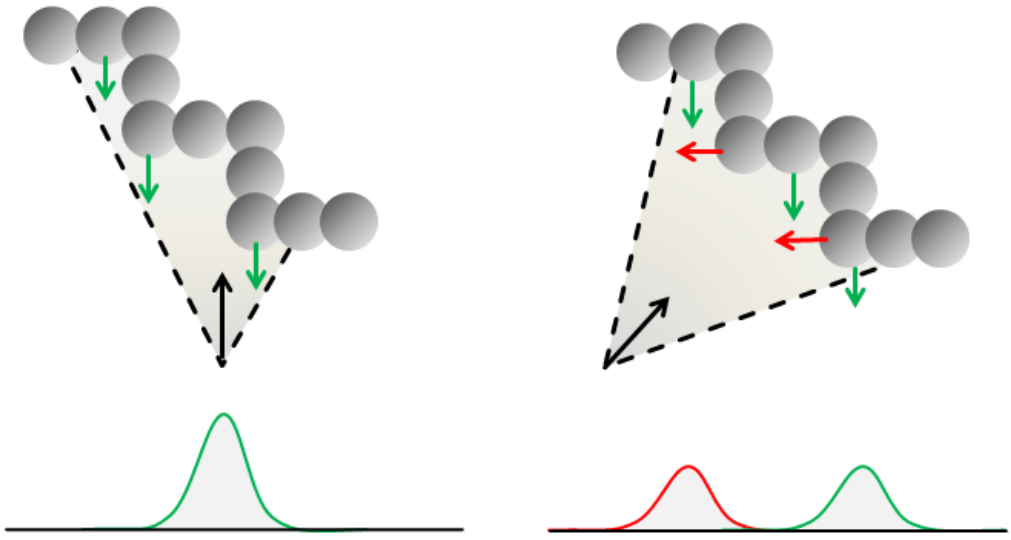

Figure 4.1: The changing distribution of visible normals under changing view directions of a v-groove surface consisting of just a few particles. While under certain view directions (left) an approximation of the normal distribution by fitting a single normal vector would be appropriate, other view directions (right) have more complex normal distributions that cannot be represented by a single normal.

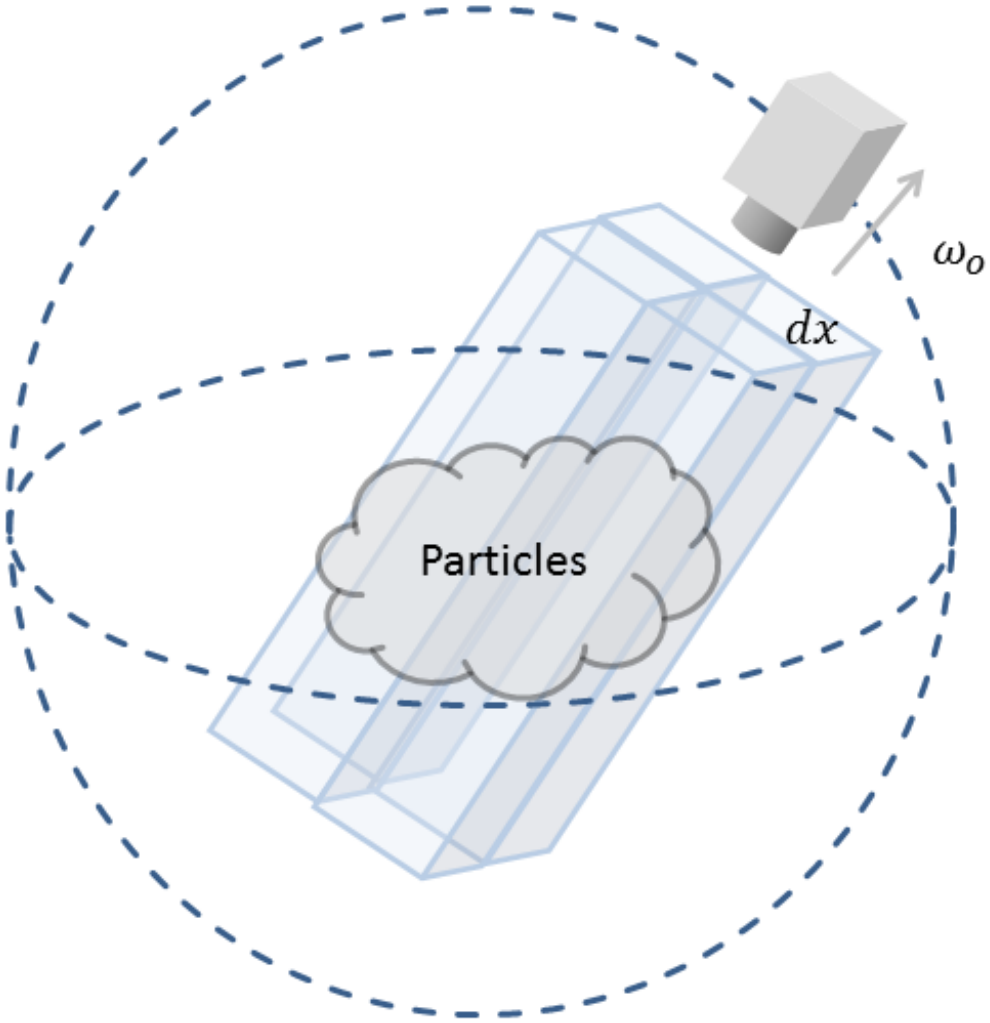

Figure 4.2: Sampling approach of a spatially varying normal distribution function of particle-based data. The camera orbits around the particle-based data sampling the distribution of visible surface normals for areas on the view plane.

Our goal is to capture the complex lighting behavior of different micro-structures that changes under different view directions. On these surfaces filtering of normal vectors play an important role. While surfaces with normal vectors that tend toward a common direction can be approximated by fitting a single normal vector, a more complex function would not be appropriately represented by a single normal vector. This is illustrated in in figure 4.1. Linearly filtering the sampled normal vectors to a

single normal vector therefore would not capture the surface correctly in most cases. In extreme cases it could even lead to singularities when attempting to apply a linear filter to oppositely pointed surfaces which results in the zero vector.

Therefore this work introduces a technique that overcomes this problem with the use of normal distribution functions as introduced in [Fou92]. Similar to classical imposters that store pre-computed images of certain view directions the approach introduced in this chapter stores statistical information about the visible particle surfaces that can be directly used during shading without requiring the original particle-based data.

Normal distribution functions are defined on the tangent frame of the local geometry (section 2.1.4). However, particle-based data do not have topology thus do not form surfaces on which local tangent frames could be defined.
To overcome this problem we define the NDFs on the visible surface projected on the view plane. This way the tangent frame is the view plane itself. We account for the changing view planes and masking under different view directions by extending the NDF to be view-dependent. The resulting view-dependent NDFs are four-dimensional functions that spatially vary over the output resolution pixels rather than over the particle surface leaving the rendering performance independent of the particle data complexity.

For each area dx on the view plane orthogonal to the view direction ω_o the view dependent normal distribution function $NDF(\omega_o, \omega_i)$ is defined by the amount of projected particle surface area oriented along the given normal vector ω_i visible under view direction ω_o. The NDF is a probability distribution hence $\forall\omega_o : \int_\Omega NDF(o,i)(o{\cdot}i)\omega_i = 1$. To fulfill this requirement the NDF has to be appropriately normalized. It is important to consider the projected area of the normal i on the tangent frame normal o. and account for the amount of area on which there is no projected particle surface at all.

The process of computing the normal distribution function is similar to the way a gonioreflectometer works. A material sample is inspected under various view directions by orbiting the camera around the sample. The spatial variation on the imposter is addressed using displacement in the view plane. In contrast to measuring BRDFs not the relation of incident to outgoing light is measured but rather the contribution of each normal vector to the total shading. This process is illustrated in figure 4.2. An NDF imposter therefore is a six-dimensional function where two dimensions correspond to the spatial position on the view plane, two dimension to the normalized view vector and the remaining two dimensions to the normalized normal vector.

4.2 Pre-processing

In a pre-computation step the input particle-based data is transformed into an NDF imposter with a given target output resolution and standard mip mapping. Rendering of the resulting NDF imposter neither requires the original particle-based data nor assumes a fixed shading model.

4.2.1 Data structure

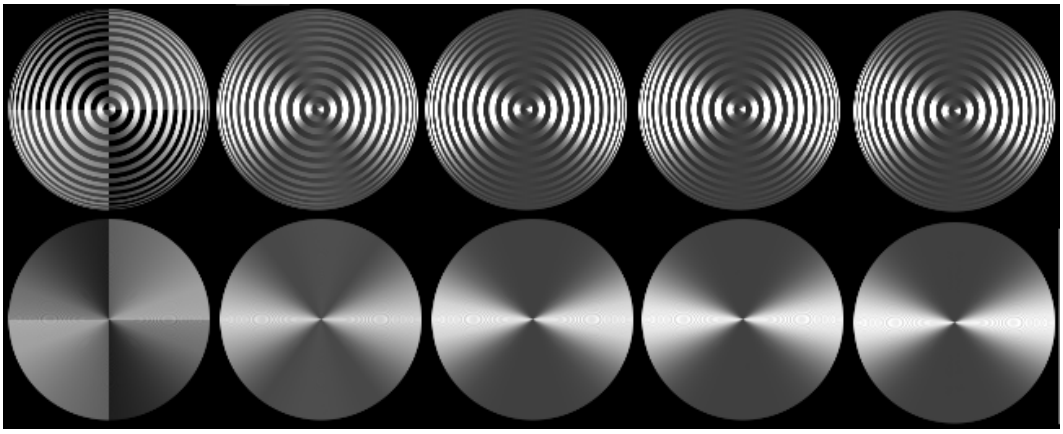

Figure 4.3: Comparison of the effect of different amounts of histogram bins on the visual quality. A synthetic dataset of radial v-grooves resembling radially brushed metal is rendered using the NDF imposter with increasing amounts of histogram bins. Starting with 4x4 bins on the left doubling up to 32x32 bins on the right. As little as 8x8 histogram bins is sufficient to have convincing visual quality and mainting of the anisotropic shading of sub-pixel features.

Similar to classical imposters, NDF imposters are two-dimensional in the spatial domain but instead of a shading result they contain per-pixel normal distribution functions describing the underlying particle surfaces. The imposter resolution is aimed to fit the output resolution.
An individual NDF is represented as a four-dimensional histogram using a single-precision floating-point array where two dimensions are used for the normalized view vector and the other two dimensions for the normal vector discretizations. Therefore the NDF imposter is stored as a contiguous six-dimensional grid in main memory and as-is in a shader storage buffer object in graphics memory.
Evaluation of an NDF given the normalized view and normal vector is done by simply sampling the nearest histogram bin value as done in the code sample 4.1. Alternatively

neighboring values can also be interpolated.

```
ndfLookup(vec3 view, vec3 normal) {
      return ndf[int(view.y * Res)][int(view.x * Res)]
            [int(normal.y * Res)][int(normal.x * Res)];
}
```

Listing 4.1: Code sample of an NDF evaluation of a given set of normalized view and normal vectors. Res is the resolution of the discretization.

Experiments have shown that even small numbers of histogram bins as small as 8x8x8x8 deliver good visual results and reasonable memory consumption, leaving current, more elaborate methods like von Mises-Fisher distributions [HSRG07] as an opportunity to target higher output resolutions and as ab optimization of rendering performance. A comparison of different histogram sizes is shown in figure 4.3 using a synthetic dataset. Another possibility to simplify the model is the assumption of a fixed view direction and orthographic projection under which the view direction is fixed, reducing the NDFs to two-dimensional functions which can be helpful for fast pre-computations with a fixed camera.

4.2.2 Tiled Rendering

Sets of particles represented by their three-dimensional position are loaded from either a MegaMol particle file (.mmpld) [GKM+14] or are synthetically generated on startup. For simplicity a global particle radius is used, although this approach is not limited to equally-sized or identically-shaped glyphs.
Screenspace tiling is done by modifying the projection matrix to only cover the frustum covered by the target pixel. This way a tile for each output resolution pixel is calculated independently. Variation of the view direction is achieved by orbiting the camera around the sample.

4.2.3 Normal Sampling

The visible normals in each tile are sampled using a modified direct particle rendering technique based on the approach described in section 2.1.1. The particle renderer is modified in a way that it renders the view-space normal vectors into a render buffer instead of the shaded result. Standard depth testing is used to only leave the visible normals for the following binning step. Numerical problems are reduced as well as avoiding the need for distorting particles to ellipses by the use of an orthographic projection because all rays of the pixels are parallel.

The sampling rate per tile is set by the user and is assumed to be large enough to appropriately capture the particles' surface normals. The size of the smallest particle glyph and target output resolution have to be considered when choosing the sampling rate. If the sampling rate is too low, aliasing will occur due to the same under-sampling issues as direct particle rendering suffers from. Besides under-sampling, numerical errors limit the maximum amount of samples that can be taken accurately when using screen-space tiling. Large values of particle positions against very small world space pixel footprints are prone to numerical error. This problem is considerably worse when using a perspective projection. The resulting noise in samples generates randomly distributed normal vectors. One way to address this problem is by avoiding screen-space tiling altogether and instead transform the particles in a way that only the particles within the frustum of the sampling tile are visible. This way the projection matrix remains the same for each tile, leaving the world-space pixel-footprints within an appropriate scale.

The pre-computation is expensive though tiles can be calculated independently and parallelizable by image-space decomposition. Thereby the computation can be easily distributed on compute clusters, multicore and multi GPU machines. Additionally hardware rasterization is used and well-suited for rendering large amounts of particles in the same way as for the state-of-the-art direct particle rendering in the first place.

4.2.4 Binning

Based on the accurately sampled visible normal vectors, NDF representations can subsequently be computed for each tile. In the case of histograms this is a simply iteration over the render buffer that quantizes the normal vectors into histogram bins and increments the bin values. Once all normal vectors are binned the histogram has to be normalized to integrate to one resulting in a valid PDF. However rays not hitting any particle do not result in valid normal vectors and have to be filtered out before binning. To account for those invalid normal vectors the histogram is normalized in a way that the integral represents the ratio of rays hitting a particle over the total amount of rays. This is important to correctly represent sparsely populated regions. Since normal distribution functions can be filtered linearly, all coarser mip levels are computed bottom up from the finest-resolution level by repeatedly combining the data into the next lower resolution level using a bilinear filter. This process is repeated iteratively until the coarsest mip level is reached. This way a single NDF can be computed for the whole dataset.

4.3 Rendering

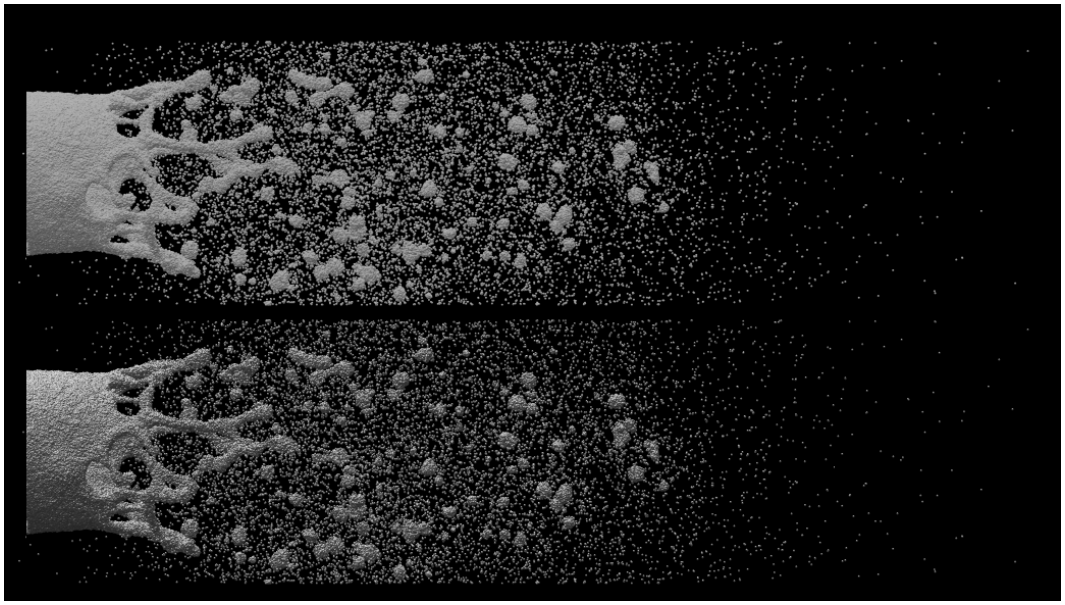

Figure 4.4: Comparison of a Lambert (top) and Phong (bottom) glyph BRDF.

Rendering of the imposter takes place in a fragment shader applied to the view-aligned billboard 2.1.2. For each fragment on the imposter we can easily calculate the spatial position and view direction. This information combined with the NDF can be used to accurately evaluate a given BRDF in the fragment shader.

4.3.1 Shading

During shading each normal of each fragment is individually shaded by evaluating the BRDF and weighted by its contribution to the total fragment shading result by evaluating the NDF. The difference between the Lambert and Phong BRDF is shown in figure 4.4. The required normal vector can be obtained by a simple transformation of the histogram bin indices to the range -0.5 to 0.5. The third coordinate is obtained using the constant length of normalized vectors, see equation 4.1.

$$1 = x^2 + y^2 + z^2 \rightarrow z = -\sqrt{1 - x^2 - y^2} \tag{4.1}$$

Pseudo code of NDF imposter shading is provided in listing 4.2.

```
pixelOutput = 0
for j from 0 to HistogramHeight
      for i from 0 to HistogramWidth
```

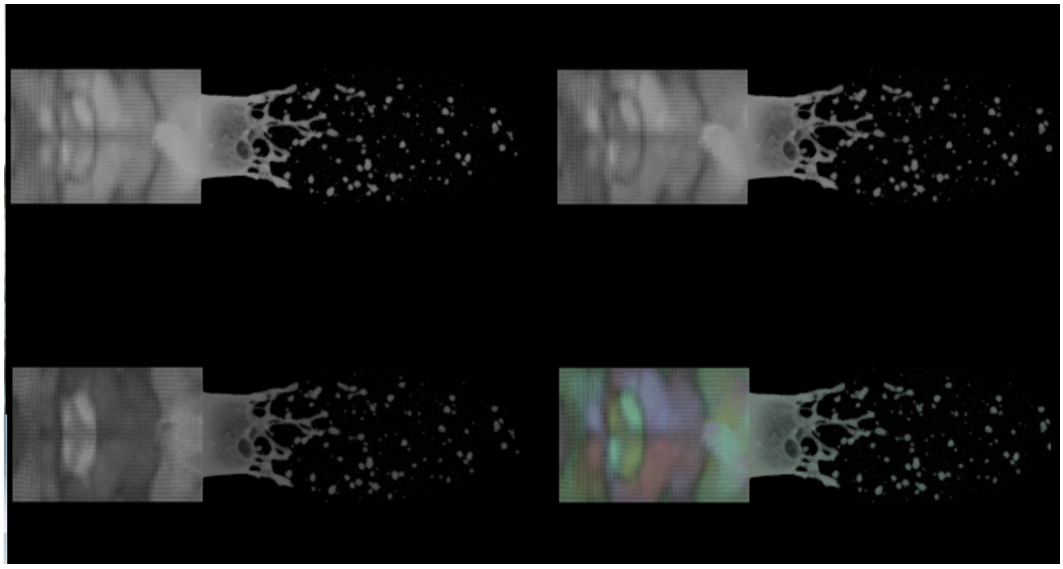

Figure 4.5: Comparison of different shading of the same NDF imposter of 48 million particles. From left to right, top to bottom: Lambert, Phong, Phong with translated light source, Colored cube environment map mixed with phong

```
x = (i / HistogramWidth) - 0.5
y = (j / HistogramHeight) - 0.5
normal = (x, y, -sqrt(1 - x*x - y*y))

shading = 0
for lightSources
      shading += BRDF(lightDirection, viewDirection, normal)

pixelOutput += NDF(normal, viewDirection) * shading
```

Listing 4.2: Shading pseudo code

An array of per-pixel NDFs and their effective BRDFs after convolution with the glyph BRDF is shown in figure 4.6. The appearance of the course per-pixel NDFs fit the highly detailed NDF shown in figure 2.1.

4.3.2 Environment mapping

Additionally knowing the contribution of each normal vector to the total shading enables accurate filtering of transfer functions evaluated on vectors depending on the normal and view vectors. Examples include the reflection vectors used in environment mapping and image-based lighting [Deb02, HSRG07] or even transfer functions on the normal vectors themselves. This can be observed in figure 4.5 where an unfiltered

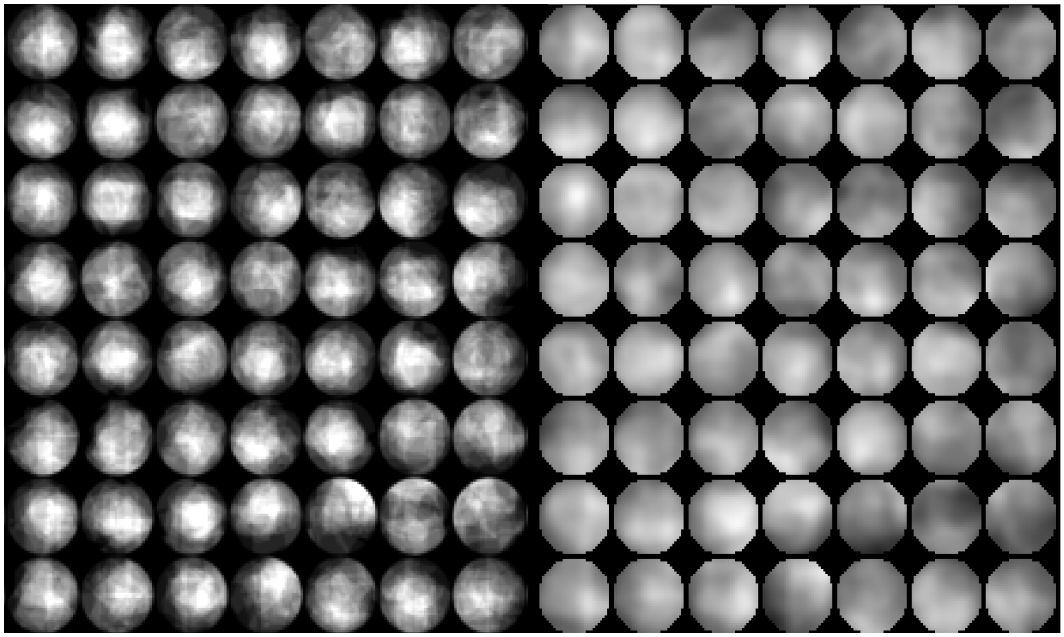

Figure 4.6: Array of neighboring per-pixel normal distribution functions on the left and their corresponding effective BRDFs resulting from a convolution with the Phong BRDF used on the individual sphere glyphs. Note that the resulting effective BRDFs are anisotropic although the glyph BRDF is not.

environment map consisting of a cube with singly-colored faces is filtered smoothly.

Using image-based lighting the sum over a discrete set of light sources can be transformed into sampling a light map allowing large amounts of light sources stored in a light map. The roughness of the surface determines how broad the reflections are. This is usually achieved by pre-filtering the light map for different amounts of roughness set by the user. If the shading is performed using the computed NDF imposter rough surface areas have broader reflection as smooth surfaces, without the need of pre-filtering the light map and requiring the user to set the roughness of surface areas as it results directly from the captured micro-scale geometry. Mirror-like surfaces areas have small peaks in their NDF resulting in sharp reflection while more glossy surface areas have wider distributions resulting in broader and smoother reflections.

Applying image-based lighting on a single normal vector per pixel is problematic because of the planar approximations of the geometry that does not capture the micro-scale geometry well. This effect is further amplified by the divergence of normal vectors of only slightly differently oriented planar approximations. Applying a linear filter to multiple samples of the environment map around the normal vector can reduce aliasing. However this does not account for the actual normal distribution and leaves

reflections on perfectly specular surfaces as too smooth and reflections on diffuse surfaces as too sharp.

4.3.3 Performance

This rendering implementation achieves real-time performance on current graphics hardware despite the large amount of BRDF and NDF evaluations required per pixel. The amount of evaluations required can be drastically reduced by relying on a more elaborate NDF representation [HSRG07] that reduces shading to convolution of continuous functions described by only a few coefficients. The same approach can also be applied to environment mapping by representing the environment map as a set of spherical harmonics coefficients or other basis functions that can be convoluted with the NDF representation like von Mises-Fisher distributions [HSRG07].

Instead of convolving the BRDF and NDFs each frame the pre-integrated effective BRDFs for a fixed glyph BRDF could be stored. This approach would only require the convolution of the glyph BRDF and NDFs if either changes. Also shading using this approach requires only a single evaluation of the effective BRDF per light source and is no longer dependent on the NDF resolution or representation in general. This requires only little computational efforts in the same order of shading a normal mapped surface but is a lot more accurate. Note that the effective BRDF typically has lower frequencies than the NDF it originates from, thus could be approximated more easily.

5 Results

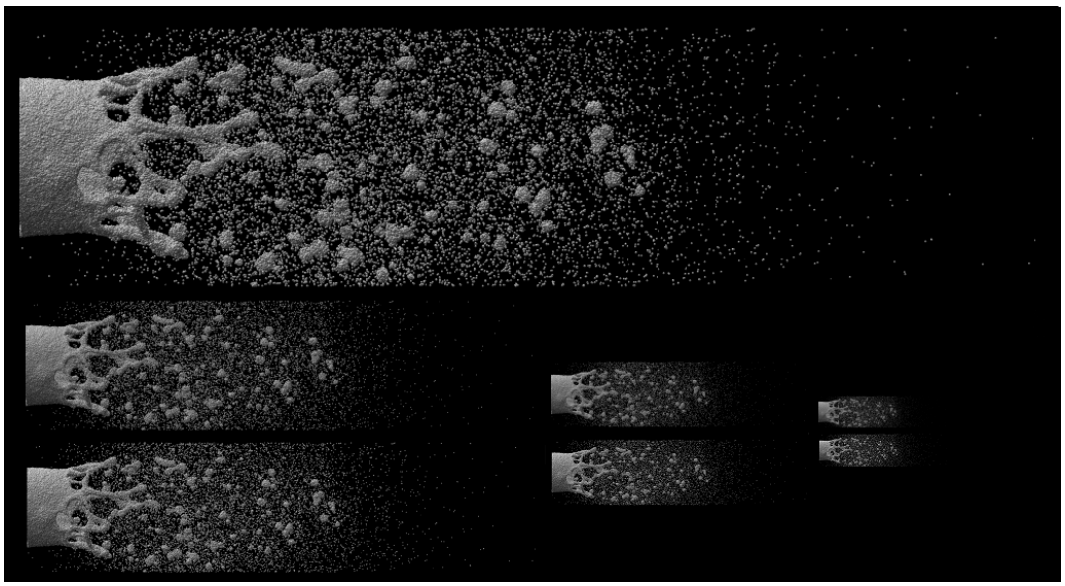

Figure 5.1: A rendering using the NDF imposter at the top and a comparison of different scales below. The upper row is rendering using different mip levels of the NDF imposter. The lower rows uses image-space downsampling of the finest resolution level of the NDF Imposter.

Precomputed NDF imposters enable high quality representation of particle-based data across all scales. Downsampling, required for mip mapping, is efficient and resistant to aliasing. A comparison of different mip levels of NDF imposter against image-space downsampling of the full resolution rendering is shown in figure 5.1. The NDF imposters perform well compared against image-space downsampling. Another example shows the preservation of the shading behavior on a synthetic dataset of a sphere with saw tooth surface features in figure 5.2. Rendering of a small dataset with the Lambert and Phong shading models is shown in figure 5.3.

Even small histogram discretizations deliver good visual quality. The consistency of the introduced technique significantly simplifies rendering particles in all scales since the user does not have worry about picking different visualization techniques for different scales or amounts of data. Also, there is no need for adjusting transfer func-

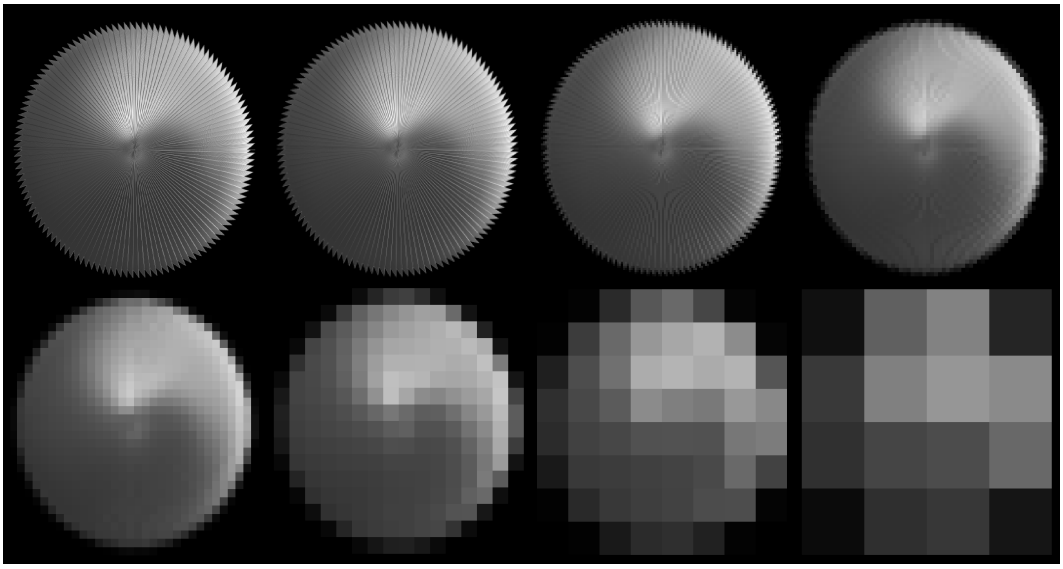

Figure 5.2: LOD levels of the NDF imposter scaled to a fixed resolution. Filtering between neighboring pixels is disabled. The shading behavior is captured accurately even on a small amount of pixels.

tions for multiple mip levels individually. The consistency throughout all scales enables high-level overviews of the small-scale surfaces. Although this approach is not free of aliasing, it reduces the effect of aliasing dramatically compared to direct particle rendering, ensuring correct representation of particles smaller than a single pixel-footprint.

Even the most rudimentary model of perfect Lambertian sphere glyphs produces suprisingly complex shading behavior on a macro-scale. The available spatially varying normal distribution function enables further applications to complex shading models, accurate environment map sampling or the use of synthetically generated transfer functions to highlight specific details like discontinuities, cracks or other features of interest.

Changing particle radii of the cross ablation dataset are shown in figure 5.4. Larger particle radii result in smoother surfaces due to larger amounts of occlusion whereby smaller radii allow the visualization of waves caused by small scale dislocations in regular grid like shock waves in metallic lattices. Those waves can be seen in the laser ablation and cross ablation datasets. However aliasing artifacts of regular grids occur, caused by the box filter used while binning the NDF histograms. Improved filtering during pre-computation and rendering that currently uses nearest neighbor interpolation could eliminate this problem.

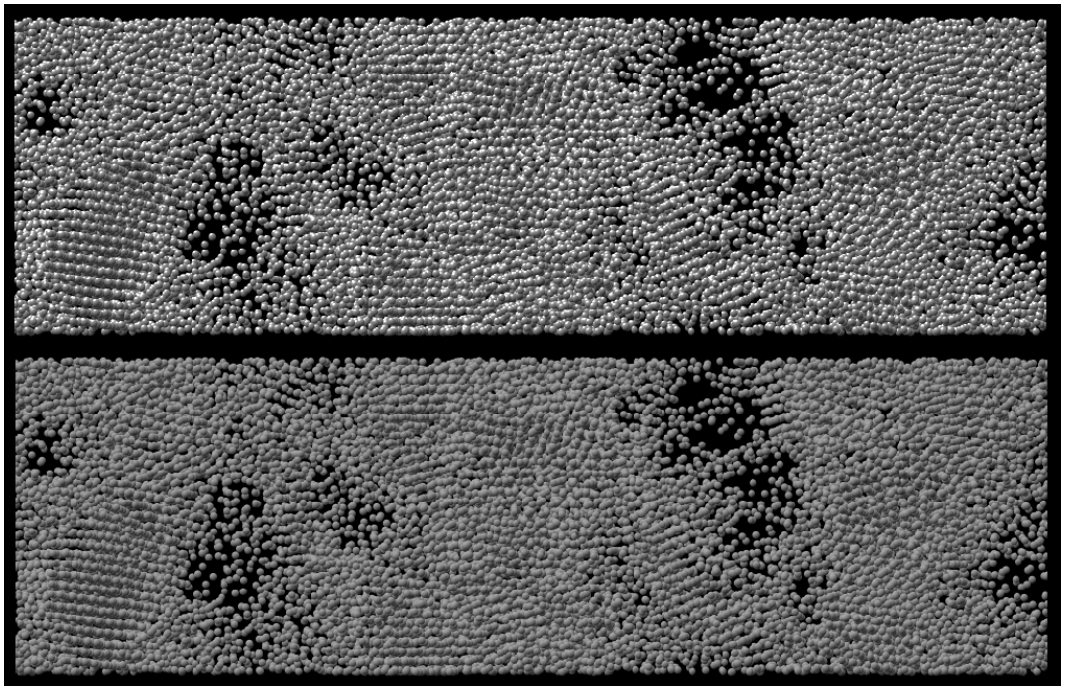

Figure 5.3: Rendering of a smaller dataset consisting of only few particles that could also be rendered using direct particle rendering without under-sampling. This shows the consistency of NDF imposters with the underlying glyph model which is accurately represented even in the micro-scale.

5.1 Problems

High memory requirements limit the application to small output resolutions or few view directions. As an example using 9x9x9x9 histograms using 4 byte single-precision floating-point values the NDF imposter requires 256x256x9x9x9x9x4 bytes = 1719926784 bytes = 1679616 kBytes = 1640 mBytes = 1.6 gBytes. This is feasible using current graphics hardware but does not scale with higher resolutions. This problem could be avoided by storing only the effective BRDFs on the graphics hardware resulting from high-resolution NDFs stored elsewhere.

Initially 2D NDF imposters described in chapter 4 were planned to be a preliminary experiment leading towards NDF volume rendering. This concept cannot be easily translated into volume rendering because of the incapability of compositing NDF voxels during volume traversal, resulting from a lack of knowledge about occlusion and selection of visible normals. While this is tolerable for direct volume rendering, linear combination of NDFs along the view ray is not acceptable since it does not take partial occlusion by the particles in the previously traversed voxel into account. In

contrast to volume rendering, classical imposters restrict the camera to be located outside of the particle domain.

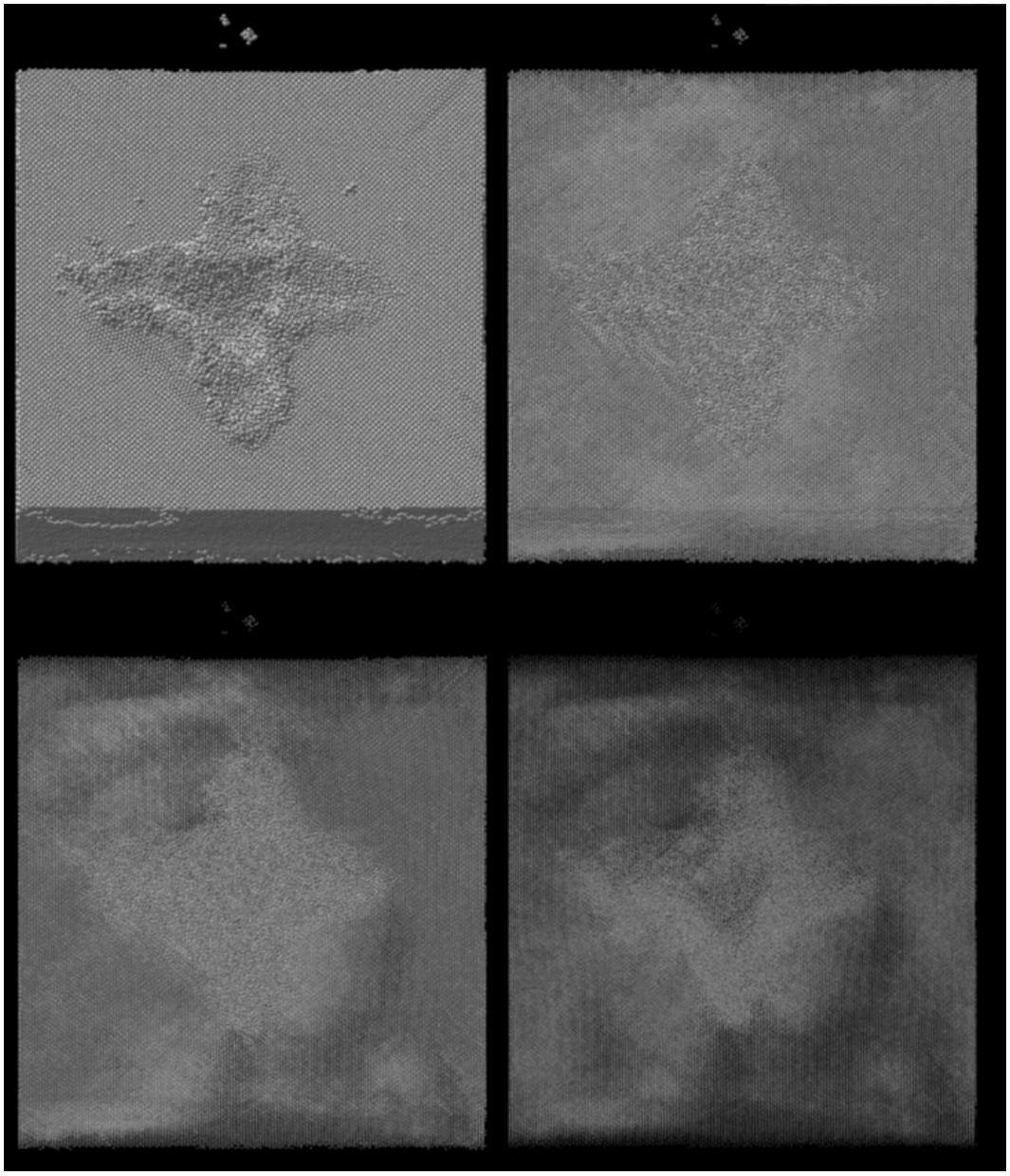

Figure 5.4: Changing radius of a cross ablation dataset. Decreasing from left to right, top to bottom. Higher radii enable better interpretation of the overall shape and cracks in the surface while small radii highlight dislocations in the solid cuboid. The darker areas do not result from density fluctuation but from low-frequent shading effects caused by dislocations in the microstructure and changes when moving the light source.

6 Conclusion and Future Work

Experiments during this work have shown complex local illumination of the presumed sphere glyph model in the macro-scale that cannot be captured using the previous techniques of direct particle rendering and mip mapped volume rendering using illumination based on the density gradient.

Direct particle rendering can only represent particles appropriately if the sampling rate fits the particle size. It relies on multiple samples per glyph unfeasible when rendering millions of particles with interactive frame rates. While this approach is a good solution for renderings in the micro-scale, it quickly degenerates to white noise due to aliasing.

Mip mapped volume rendering of density scalar fields result in smoothed particle clusters which is an inappropriate representation of the hard non-intersecting surfaces of particle glyphs. The amount of particles in smoothed clusters are not comparable or countable, making it difficult to distinguish near and far clusters.

The introduced NDF imposters enables the visualization of particle-based data at the macro-scale while being consistent with the underlying glyph model. This is important since the roughness and anisotropic shading behavior is an important feature that visually conveys information about the micro-scale structure that cannot be determined by a user upfront or set globally.

As observed in the laser ablation and cross ablation datasets irregular structures like shock waves emerge from densely-packed regular grids that would otherwise be hidden by occlusion. That led to a visualization of shock waves in the laser ablation cuboid never seen before using the sphere glyph model. This has been confirmed as truthful by the original authors of the simulation.

Overall the introduced technique can be used as ground truth rendering technique of particle-based data consisting of fully opaque surface and any local illumination model.

6.1 Future Work

Color mapping of mixtures of differently colored particles cannot be applied to this representation because it lacks information about the distribution of particle types or color information.
Downsampling of pre-classified mixtures of particle colors suffers from the same inconsistency artifacts as applying transfer functions to normal vectors do. Sparse pdf maps [HSB+12] (section 2.2.3) have shown a way to address this issue by post classifying mixtures of colored particles by preserving the histogram over all scales.

During pre-computation discontinuities could be accentuated using ambient occlusion as well as inter-reflections taken into account as done in the microfacet model [CT82].

Experiments with interpolation between neighboring view direction and histograms show promising results indicating high potential of reducing the memory requirement of the six-dimensional data using sparse approximation. Especially the NDF representation as a full histogram limits the output resolution and number of view directions NDF imposters can be used for due to exploding memory consumption. Sparse approximation of NDFs for a fixed view direction have been studied in [OB10, HSRG07, DHI+13] though all of these approaches are applied to polygonal model where a tangent frame is defined.

Furthermore the same approach could also be applied to normal mapped polygonal meshes. Instead of storing normal maps, sparse approximations of view-dependent normal distribution functions could be stored. Allowing efficient downsampling with the use of linear filters while preserving anisotropic and view-dependent lighting behavior. Any normal map can be easily converted to such a representation [Fou92]. A single normal vector can be seen as an NDF which is delta function.

Bibliography

[Bli77] J. F. Blinn. Models of Light Reflection for Computer Synthesized Pictures. *SIGGRAPH Comput. Graph.*, 11(2):192–198, 1977. doi:10.1145/965141.563893. URL http://doi.acm.org/10.1145/965141.563893. (Cited on page 14)

[CT82] R. L. Cook, K. E. Torrance. A Reflectance Model for Computer Graphics. *ACM Trans. Graph.*, 1(1):7–24, 1982. doi:10.1145/357290.357293. URL http://doi.acm.org/10.1145/357290.357293. (Cited on pages 8 and 44)

[Deb02] P. Debevec. Image-Based Lighting. *IEEE Computer Graphics and Applications*, 22(2):26–34, 2002. doi:http://doi.ieeecomputersociety.org/10.1109/38.988744. (Cited on page 34)

[DHI+13] J. Dupuy, E. Heitz, J.-C. Iehl, P. Poulin, F. Neyret, V. Ostromoukhov. Linear Efficient Antialiased Displacement and Reflectance Mapping. *ACM Trans. Graph.*, 32(6):211:1–211:11, 2013. doi:10.1145/2508363.2508422. URL http://doi.acm.org/10.1145/2508363.2508422. (Cited on pages 17 and 44)

[Fou92] A. Fournier. Normal distribution functions and multiple surfaces. In *Graphics Interface '92 Workshop on Local Illumination*, pp. 45–52. Vancouver, BC, Canada, 1992. (Cited on pages 14, 19, 29 and 44)

[GKM+14] S. Grottel, M. Krone, C. Müller, G. Reina, T. Ertl. MegaMol - A Prototyping Framework for Particle-based Visualization. *IEEE Transactions on Visualization and Computer Graphics*, 2014. doi:10.1109/TVCG.2014.2350479. URL http://doi.acm.org/10.1109/TVCG.2014.2350479. (Cited on page 31)

[GKSE12] S. Grottel, M. Krone, K. Scharnowski, T. Ertl. Object-Space Ambient Occlusion for Molecular Dynamics. In *Proceedings of IEEE Pacific Visualization Symposium 2012*, pp. 209–216. 2012. doi:10.1109/PacificVis.2012.6183593. URL http://doi.acm.org/10.1109/PacificVis.2012.6183593. (Cited on page 8)

[GRDE10] S. Grottel, G. Reina, C. Dachsbacher, T. Ertl. Coherent Culling and Shading for Large Molecular Dynamics Visualization. In *Proceedings of the 12th Eurographics / IEEE - VGTC Conference on Visualization*, EuroVis'10, pp. 953–962. Eurographics Association, Aire-la-Ville, Switzerland, Switzerland, 2010. doi:10.1111/j.1467-8659.2009.01698.x. URL http://dx.doi.org/10.1111/j.1467-8659.2009.01698.x. (Cited on page 13)

[Gum03] S. Gumhold. Splatting Illuminated Ellipsoids with Depth Correction. In *Proceedings of International Workshop on Vision, Modeling, and Visualization*, pp. 245–252. 2003. (Cited on pages 10 and 13)

[HSB+12] M. Hadwiger, R. Sicat, J. Beyer, J. Krüger, T. Möller. Sparse PDF Maps for Non-linear Multi-resolution Image Operations. *ACM Trans. Graph.*, 31(6):133:1–133:12, 2012. doi:10.1145/2366145.2366152. URL http://doi.acm.org/10.1145/2366145.2366152. (Cited on pages 17, 23 and 44)

[HSRG07] C. Han, B. Sun, R. Ramamoorthi, E. Grinspun. Frequency Domain Normal Map Filtering. *ACM Trans. Graph.*, 26(3), 2007. doi:10.1145/1276377.1276412. URL http://doi.acm.org/10.1145/1276377.1276412. (Cited on pages 16, 31, 34, 36 and 44)

[IKLH] M. Ikitis, J. Kniss, A. Lefohn, C. Hansen. GPU Gems Chapter 39. Volume Rendering Techniques. URL http://http.developer.nvidia.com/GPUGems/gpugems_ch39.html. (Cited on page 22)

[KWN+14] A. Knoll, I. Wald, P. A. Navrátil, A. Bowen, K. Reda, M. E. Papka, K. Gaither. RBF Volume Ray Casting on Multicore and Manycore CPUs. *Comput. Graph. Forum*, 33(3):71–80, 2014. doi:10.1111/cgf.12363. URL http://dx.doi.org/10.1111/cgf.12363. (Cited on page 8)

[OB10] M. Olano, D. Baker. LEAN Mapping. In *Proceedings of the 2010 ACM SIGGRAPH Symposium on Interactive 3D Graphics and Games*, I3D '10, pp. 181–188. ACM, New York, NY, USA, 2010. doi:10.1145/1730804.1730834. URL http://doi.acm.org/10.1145/1730804.1730834. (Cited on pages 17 and 44)

[PRV13] J. Parulek, T. Ropinski, I. Viola. Seamless Visual Abstraction of Molecular Surfaces. In *Spring Conference on Computer Graphics*. 2013. Second Best Paper Award. (Cited on page 16)

[SKMH14] R. Sicat, J. Krüger, T. Möller, M. Hadwiger. Sparse PDF Volumes for Consistent Multiresolution Volume Rendering. In *IEEE Vis*. 2014. (Cited on page 17)

[SLS+96] J. Shade, D. Lischinski, D. H. Salesin, T. DeRose, J. Snyder. Hierarchical Image Caching for Accelerated Walkthroughs of Complex Environments. In *Proceedings of the 23rd Annual Conference on Computer Graphics and Interactive Techniques*, SIGGRAPH '96, pp. 75–82. ACM, New York, NY, USA, 1996. doi:10.1145/237170.237209. URL http://doi.acm.org/10.1145/237170.237209. (Cited on pages 13 and 19)

[YHJ+14] L.-Q. Yan, M. Hašan, W. Jakob, J. Lawrence, S. Marschner, R. Ramamoorthi. Rendering Glints on High-resolution Normal-mapped Specular Surfaces. *ACM Trans. Graph.*, 33(4):116:1–116:9, 2014. doi:10.1145/2601097.2601155. URL http://doi.acm.org/10.1145/2601097.2601155. (Cited on pages 11 and 15)

All links were last followed on January 8, 2015.

Declaration

I hereby declare that the work presented in this thesis is entirely my own and that I did not use any other sources and references than the listed ones. I have marked all direct or indirect statements from other sources contained therein as quotations. Neither this work nor significant parts of it were part of another examination procedure. I have not published this work in whole or in part before. The electronic copy is consistent with all submitted copies.

---

place, date, signature